USE OF LEAPFROG GEOTHERMAL SOFTWARE IN DATA INTEGRATION AND 3D VISUALIZATION CASE STUDY OF OLKARIA DOMES GEOTHERMAL SYSTEM

[1]Risper Kandie, [1]Pearce Mbuthia and [2]James Stimac

Kenya Electricity Generating Company (KenGen)
rkandie@kengen.co.ke and pmbuthia@kengen.co.ke

[2]Stimac Geothermal Consulting
sgcgeo00@gmail.com

ABSTRACT

Olkaria Domes is one of the seven (7) geothermal sub-sectors of Greater Olkaria Geothermal area (GOGA). It is still under development with current generation capacity of about 197.8 MWe from Olkaria IV Power plant and well head generating units. This figure is expected to increase when construction of Olkaria V with an installed capacity of 150 MWe is completed by 2018. Over 100 geothermal wells have been drilled that includes production and reinjection/injection wells. Various surface and subsurface data types have been used to generate a model. This paper demonstrates the capabilities of Leapfrog Geothermal Software© which has been used to creSate a 3D model of Olkaria Domes using the data from the drilled geothermal wells. The software has allowed creation of 3D model from integration of geological (borehole lithology logs and hydrothermal alteration minerals), geophysics (resistivity), discharge geochemistry (chloride, sulphate and bicarbonate concentration), geographic information systems (GIS) (maps, images and well locations) and reservoir data (formation temperature, enthalpy).
The 3D model resulting from the data integration shows that up flow zones are not localized but rather widespread and occurs in a few localities such as within OW-914, OW-915 and OW-916, OW-921A, and OW-901. Downflow/outflow zones occur within vicinities of OW-907, OW-904, OW-905 and OW-902B. The location of the upflow, downflow/outflow zones are influenced by permeability ensuing from mapped geological structures and deep intrusion. The 3D model is a useful tool for visualization thereby creating an understanding of Olkaria Domes geothermal system for better management.

Keywords: Olkaria Domes, 3D modeling, geology, temperature, alteration, structure, conceptual model, visualization, permeability, flow patterns

1.0 INTRODUCTION

1.1 The Joint UNEP-ICEIDA 3D Geologic Modeling Project

In 2015 the United Nations Environmental Program (UNEP), the Icelandic International Development Agency (ICEIDA), and the Nordic Development Fund (NDF) supported training and guidance on 3D geological model development using Leapfrog Geothermal Software©. The training program introduced the software, basic skills in data analysis and conceptual modeling, and outlined a workflow for making 3D models of geothermal systems. A total of eight (8) participants comprising geoscientists and geomaticists from Kenya and Ethiopia successfully completed the training and built initial 3D models of the Tendaho, Aluto, Menengai, and Olkaria Domes geothermal systems. The basic principles of planning deviated wells and estimating resource size from the temperature model were also covered.

In a cooperative effort, UNEP acquired a multi-user license of Leapfrog Geothermal software© for the project, while ICEIDA sponsored the training of participants representing Ethiopia Electric Power (EEP), the Geological Survey of Ethiopia (GSE), Kenya Electricity Generating Company Limited (KenGen), and Geothermal Development Company (GDC). The main objective of training program was to enable the selected professionals from Kenya and Ethiopia to develop the skills needed to build 3D conceptual models, and apply those skills to make initial models of geothermal systems in their respective countries using state-of-the-art software. A secondary goal was to develop a core group of proficient conceptual modelers in Africa that would continue to improve their skills and train others in the region.

Experienced modelers provided training in the following three (3) phases:

1) Pre-training support that included; mentoring, assistance with organizing data for input to Leapfrog, preparation of workflows
2) 10-day training workshop in Ethiopia that emphasized hands-on experience using the Leapfrog Software. This involved integrating the collected data and developing a conceptual model of the system using the software. At the end of the training participants had been exposed to the methods and approaches that are used in generating useful geothermal models in Leapfrog and had a start on preparing models of their selected geothermal systems. The approach employed is described more fully in Stimac and Mandeno (2016).
3) Post-training guidance focused on further model development and guidance, probabilistic resource size estimation, and well planning.

After the training it was expected that the participants had acquired knowledge in:

1) Operating the Leapfrog software (setting up a project, importing data,image files, point sets, etc.);
2) Collecting and integrating relevant geothermal data for use in the Leapfrog software;
3) Developing a conceptual model of a geothermal system; and
4) Understanding the basic philosophy of planning wells in Leapfrog.

1.2 Geological Setting

The Kenyan segment of the East African Rift hosts many geothermal systems, including the Greater Olkaria Geothermal Area (GOGA), the largest operating geothermal field in Africa, and one of the largest in the World currently generating<600 MWe from several sectors, including Olkaria Domes (Figure 1).

The Greater Olkaria Volcanic Complex is a young ~1.78 to <20ka), small-volume, multi-vent system dominated by peralkaline rhyolite domes and lavas (Clarke et al., 1990; Marshall et al., 2009). The youngest lava flow at Ololbutot is only about 180 years B.P. based on ^{14}C dating (Clarke et al., 1990). Within the Domes area; the Plateau, Broad Acres and some Arcuate Domes have ages of <20 ka (Marshall et al., 2009), and thus likely that some active magma bodies still underlie the area (Figure 1). Surface mapping identified the Olkaria volcanic area as a remnant of an old caldera complex that has subsequently been cut by N–S normal faulting. The faults provided the loci for later eruptions of rhyolitic domes and tephra aprons overlying each magmatic source region.

The origin of the peralkaline rhyolitic magmas is somewhat controversial, but it is likely that they generated in relatively small batches, mainly by crystal fractionation, with some contribution of crustal assimilation at shallow depths of ˷ 6 km (Marshall et al., 2009). These various magma bodies and cooling intrusions provide multiple heat sources underlying the major silicic centers distributed throughout the field. The magmatic system is thought to consist of numerous independent intermediate to silicic intrusions thought to be fed by mafic recharge, forming a zone of trachytic crystal mush (70-80% crystals) with overlying comenditic caps forming from expulsion of residual liquids (Marshall et al., 2009). Geobarometry suggests that multiple magma bodies reside at depths of 5-6 km.

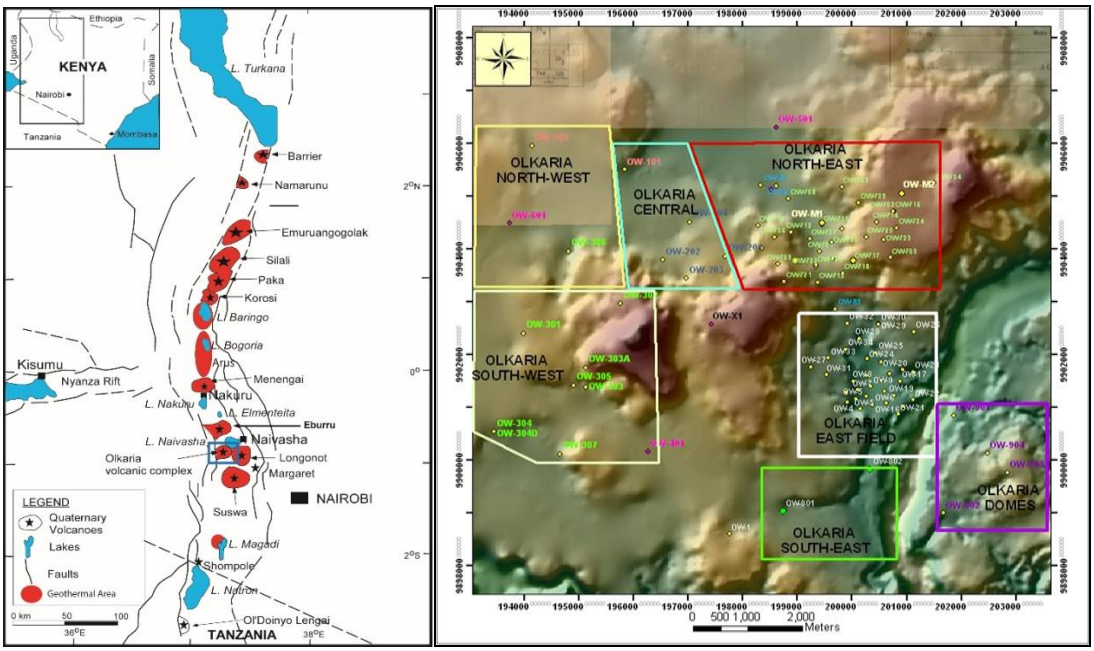

Figure 1: Location maps for geothermal areas of Kenya (left) and production sectors of the Greater Olkaria Geothermal Field (right) with Olkaria Domes highlighted in Purple.

Some of the volcanic centres are aligned on an arcuate structure that suggests that the Olkaria complex is a remnant of an older trapdoor caldera or sag structure (Mungania, 1992) (Figure. 2). Although the arcuate alignment of domes has been used to suggest the presence of a buried caldera, no major ash-flow eruptions are recognized as emanating from it, and the petrogenesis of eruptions in the last 20 ka do not support the existence of a single, large magma body (Marshall et al., 2009). The location of the Ol'Njorowa gorge is probably controlled by an important structural feature that separates the Olkaria East field from the Olkaria Domes field.

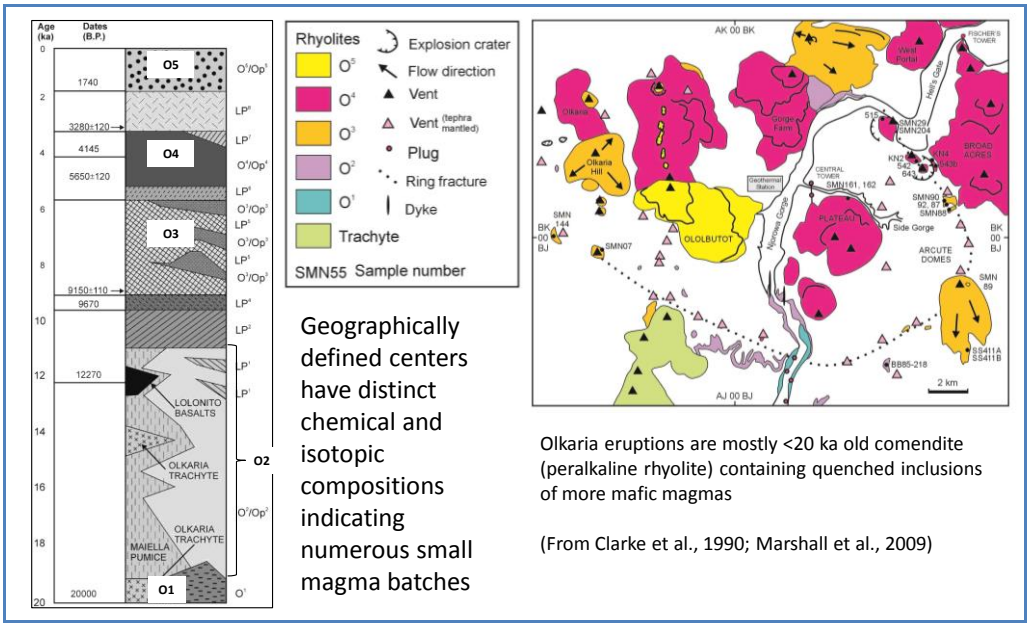

Figure 2. Olkaria volcanic vents, stratigraphic sequence, and unit ages from Marshall et al. (2009).

1.3 Geothermal Exploration History of Olkaria domes

The distribution of limited fumarolic activity is concentrated along the ring structure on the eastern side of the field and along the N-S trending fault (Clarke et al., 1990; Mungania, 1992; Kanda, 2011b). The scarcity of thermal features on the surface led to the perception that the sector was not geothermally active until Joint Geophysical Imaging (JGI) studies were undertaken in the 1990's. These surveys showed a similar resistivity structure to other productive portions of the field.

Detailed geological, geophysical and geochemical work was conducted in the area by different researchers (e.g., Mungania, 1992), and Lagat (2010) describes early exploration of the area. Surface exploration of the Olkaria Domes field was conducted in the period 1992-1993 including geophysical, geological and geochemical surveys. This led to the development of a working model and drilling of three (3) wells (OW-901, 902, 903) in June 1998 to June 1999.

The first three (3) exploration wells were drilled to a depth of ~2200 m in the western half of Olkaria Domes. They all encountered a high-temperature system and were capable of production, but hydrothermal alteration and well testing indicated a cold zone between 900-1150 m. Discharge tests showed that the wells produced a mixed $NaCO_3$–Cl–SO_4 water type with dilute chloride concentrations ranging from 178 to 280 ppm (Opondo, 2008). Productivity and permeability of the wells was low compared to wells drilled in the Olkaria East and Olkaria North East fields. The analyses of well completion tests and alteration mineralogy indicated that the resource was deeper compared to the other sectors of Olkaria.

Six (6) appraisal wells OW-903A, OW-904A, OW-905A, OW-906A, OW-907A and OW-908 were recommended to delineate the geothermal reservoir and also site production wells. The planned wells had production casings set at 1200 m (deeper than in other parts of the field), the termination depths were also deep in the order of 3000 m. This approach successfully isolated shallow cooler zones, and tapped deeper and hotter permeable zones. Directional drilling was later employed to target faults and fractures for enhanced permeability and increase average production. Well outputs increased from ~2.5 MWe to 8 MWe per well, with the highest production rate being >14 MWe.

1.4 Current Production Status

Currently the Olkaria Domes field is generating a total of 197.8 MWe, the installed capacity is150 MWe from the Olkaria IV plant and wellhead generators (WHG); OLK-905 (5MWe), OLK-914 (27.8 MWe), and OLK-915(10 MWe) and OLK-919 (5 MWe). Additionally, steam has been realized for the development of Olkaria V plant (140 MWe) whose ground breaking is expected late in the year 2016.The Olkaria Domes reservoir area has been delineated and is about 27 km^2 based on available data and with a likely power density varying from 10 to 15 MW/km^2, a capacity of between 270 and 405 MW is estimated as the available resource.

2.0 THE 3D LEAPFROG MODEL OF OLKARIA DOMES

The model presented here was developed in 2015 as part of a training project in the use of 3D visualization software. This model will be refined by further review of the input data, and addition of new information as it becomes available.

2.1 Data Types

The project considered a wide variety of geoscientific and reservoir data, with the goal of reviewing all the available information using a common frame of reference. This allows easier comparison and

integration of data across traditional disciplines, and facilitate consideration of possible conceptual models consistent with the data (Stimac and Mandeno, 2016).

Surface geologic data included satellite imagery and geological maps, lithology logs, borehole wellhead locations and directional survey data that were input to portray the well trajectories in 3D. Sub-surface geologic data from wells included major primary rocks and alteration types from rock cuttings samples. Geochemical data was initially restricted to well discharge sampling information such as chloride concentration, enthalpy and inferred Na/K geothermometer temperatures. Geophysical survey information included resistivity (MT, TEM), gravity (bouguer anomaly map) and magnetics.

2.1.1 Geological Data

Surface mapping and lithologic data from 65 wells were used as a basis for a stratigraphic model of the field. The large number of relatively thinly bedded lava and tuff units of similar character and composition proved to be a challenge in an attempt to correlate well to well. Generally the lithological model indicates that the top unit is a pyroclastic unit ranging in thickness from 100m to about 300m. It is followed by rhyolites with minor tuff intercalations to about 800m. The subsequent lithology is a trachyte intercalated with rhyolite and thin lenses of basalt and tuff. Finally, the deep lithology is dominated with trachytes to 3000m with occasional intrusions of syenitic and granitic composition.

Alteration mineralogy was determined from descriptions of rock cuttings by binocular observations and XRD analysis. Alteration assemblages proved to be more easily correlated and mappable from well to well. Alterations patterns appear to correlate very well with resistivity patterns. Alteration assemblages used were generated from data obtained from 33 wells. An attempt was also made to infer the trend of some major surface structures to depth.

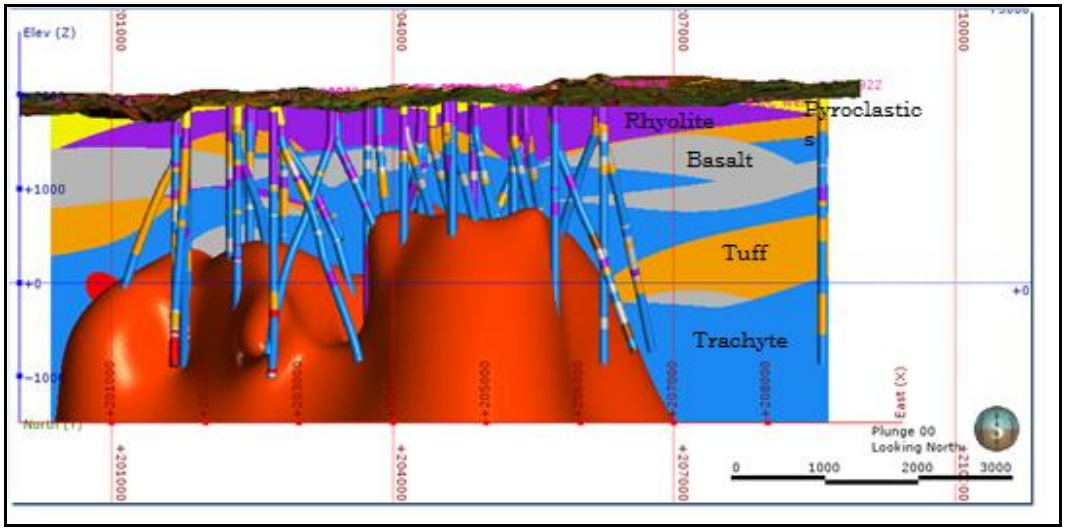

Figure 3: 3D slice of major stratigraphic units and interpolated reservoir temperature from well profiles. Also illustrated is lithology painted on each well trajectories. Not all wells shown are in the plane of the pictured model.

2.1.2 Hydrothermal Alteration Model

Study of well cuttings (typically sampled at 2 m intervals) has been used to define a number of hydrothermal alteration zones that formed at progressively higher temperatures (e. g. Lagat et al, 2005 and Atieno, 2011). In a typical model (Table 1) the youngest volcanic deposits are unaltered. Low-temperature smectite or mixed-layer clay-zeolite alteration usually occurs below this, grading into Chlorite-Illite alteration. Temperature profiles show that the low temperature clay-rich zone in wells corresponds to a region of high conductive gradient, forming the top seal on the reservoir. The reservoir

zone of wells most closely corresponds with propylitic alteration subdivided into Epidote-Illite-Chlorite and Epidote-Actinolite bearing assemblages. Garnet and biotite are sparingly encountered along with actinolite in the deepest and hottest wells, signaling proximity to intrusions. An E-W cross section showing alteration zones in the vicinity of wells OW-917 to OW-902 (west to east) is shown in Figure 4. Correlation of the alteration zones and temperature profiles generally shows that the observed alteration is in approximate equilibrium with measured temperatures, with some local exceptions (e.g., Lagat et al, 2005).

Table 1. Alteration Zones in OW-914 (from Atieno, 2011).

Depth (m)	**Key Alteration Minerals**	**Approximate Temperature range (°C)**
0-200	Unaltered	<50
200-315	Smectite-Zeolite	50-200
315-840	Chlorite-Illite (Mixed layer clays)	200-240
840-950	Epidote-Illite-Chlorite	240-280
950-2900	Epidote-Actinolite (Garnet-Biotite)	>280

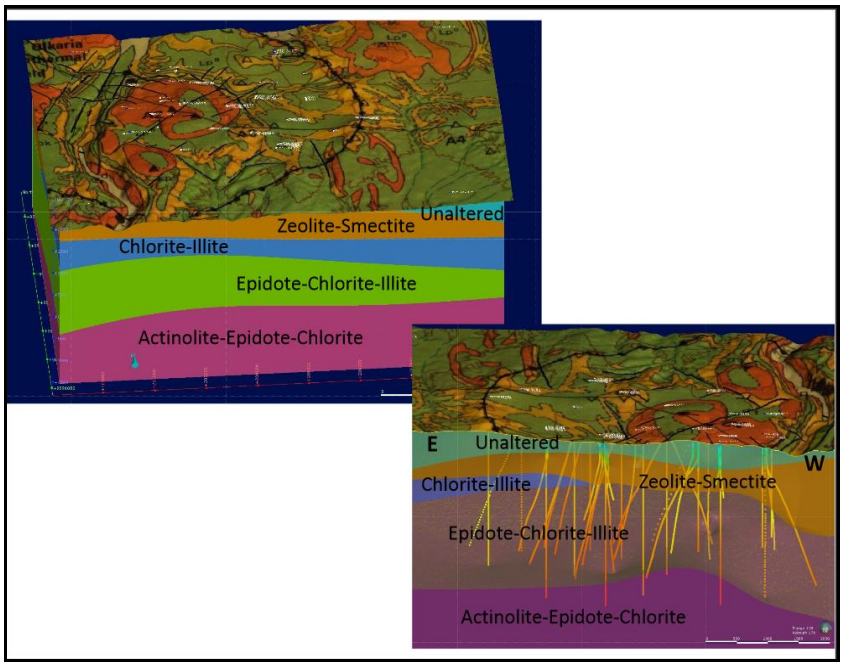

Figure 4: Cross section along W-E direction showing alteration zones. Unaltered rocks are shown in orange.

2.1.3 Geophysical Data

The main import of geophysical data was in the form of interpreted resistivity maps and cross sections. The resistivity maps and cross sections were generated from joint inversions of MT and TEM soundings Figure 5. The main use of this data set is to better understand the distribution of shallow smectite-rich clay alteration zones that may be related to underlying geothermal system. Resistivity consistent with typical propylitically altered volcanic rocks were also considered for interpretation of the extent and geometry of the reservoir zone. Since wells have already been drilled throughout the area, comparison of resistivity and observed alteration was possible, and largely validated experience with the correlation of alteration type and resistivity from other areas (e.g. Ussher et al., 2000). An example of comparison of resistivity, alteration, and measured temperature is shown in Figure 6.

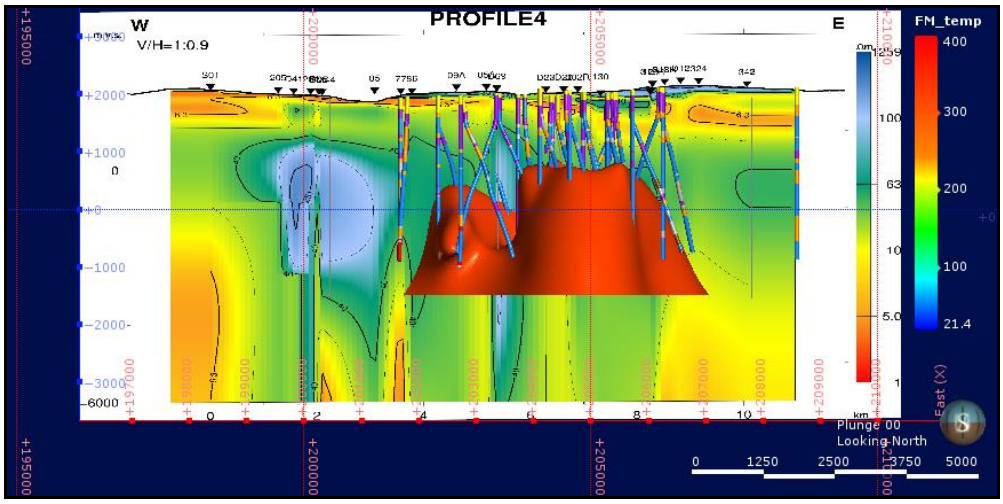

Figure 5: E-W slice viewed looking N of temperature isosurface>300°C (orange), wells with stratigraphic units, and resistivity Profile 4.

2.1.4 Resistivity Patterns

Comparison of well data to 1-D joint inversion results indicate resistivity patterns generally correlate with the type and intensity of hydrothermal alteration. Resistivity patterns include a shallow high-resistivity zone (>100 ohm-m) to about 300 m below the surface, a low resistivity zone (10 ohm-m) to depths of about 1 km and a deeper high-resistivity zone (>50 ohm-m), up to 3-4 km depth (Lichoro, 2009). A reasonably good correlation is found between the resistivity structure, hydrothermal alteration and reservoir temperatures measured in wells. High resistivities measured near surface are in areas of young volcanism with little alteration. The underlying low resistivity zone is dominated by conductive minerals comprising smectite-zeolite alteration at temperatures of 100-200°C. In the temperature range of 200-240°C, zeolites disappear and smectite is gradually replaced by more resistive chlorite. At temperatures exceeding 250°C, chlorite and epidote are the dominant minerals and the resistivity is probably dominated by the pore fluid conduction in the high-resistivity core, provided that hydrothermal alteration is in equilibrium with the present temperature of the reservoir (Lichoro, 2009).

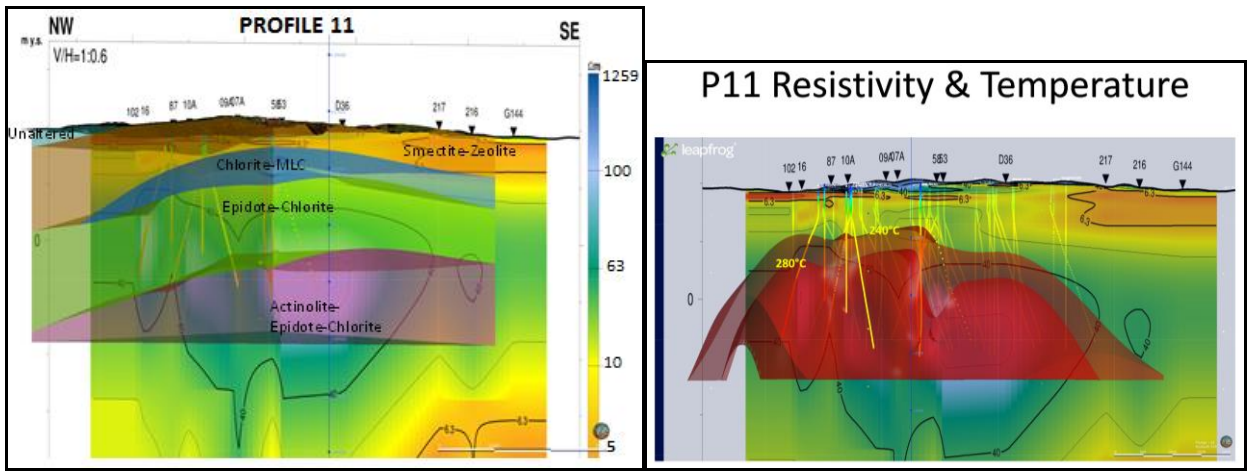

Figure 6. Comparison of alteration zones, resistivity, and interpolated measured temperature along 3D slices centered on resistivity Profile 11 (SW-NE).depth scale not clear/not shown

2.1.5 Geochemical Data

Well discharge samples were collected at 1 bar absolute in a weir box, and therefore do not fully represent reservoir conditions. Standard sampling procedures for geothermal waters were observed, and major cation and anion concentrations (Na, K, Si, Cl, SO_4, and Cl) were determined. The Na-K geothermometer of Giggenbach (1988) was used to provide an additional indication of reservoir temperature.

For some wells, steam was sampled using a mini-separator (e.g., Malimo, 2009). For these samples, the deep fluid composition was calculated from the liquid sample (collected at atmospheric pressure) and the steam sample (collected at 1.2-7 bars), it was necessary to recalculate the steam sample composition to atmospheric pressure. The atmospheric steam composition was combined with the liquid sample composition in the computation of the deep fluid composition using the WATCH program V2.1 (Arnórsson and Bjarnason, 1994).

Na-K geothermometers plotted Figure 7, has been computed from 40 wells. It indicates that the reservoir temperature is more elevated in the central to lower south east zone of the domes sector corresponding to Upflow zones. Deep liquid chloride is variedly distributed. Two distinct areas of high deep liquid chloride separated by NNE zone of low concentrations can be observed Figure 8.

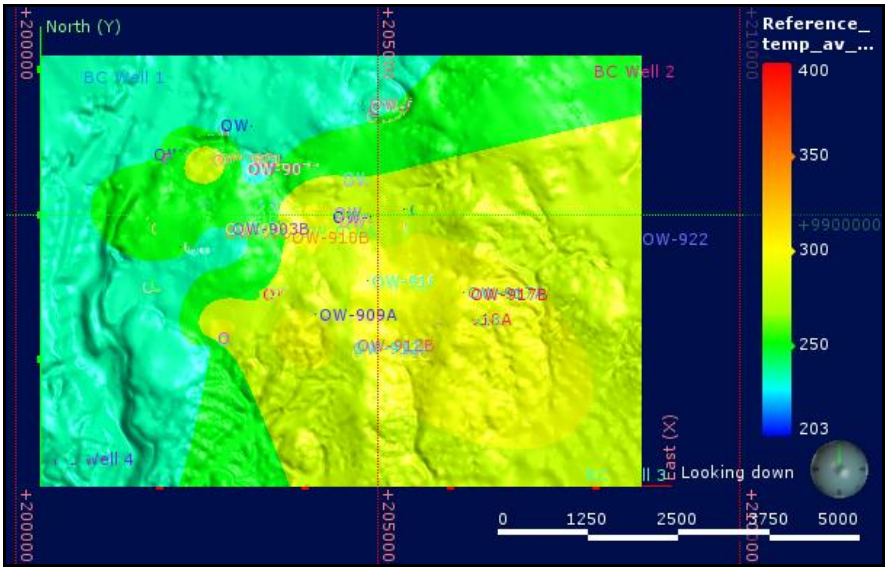

Figure 7: Interpolated reference temperature average of Na-K geothermometers.

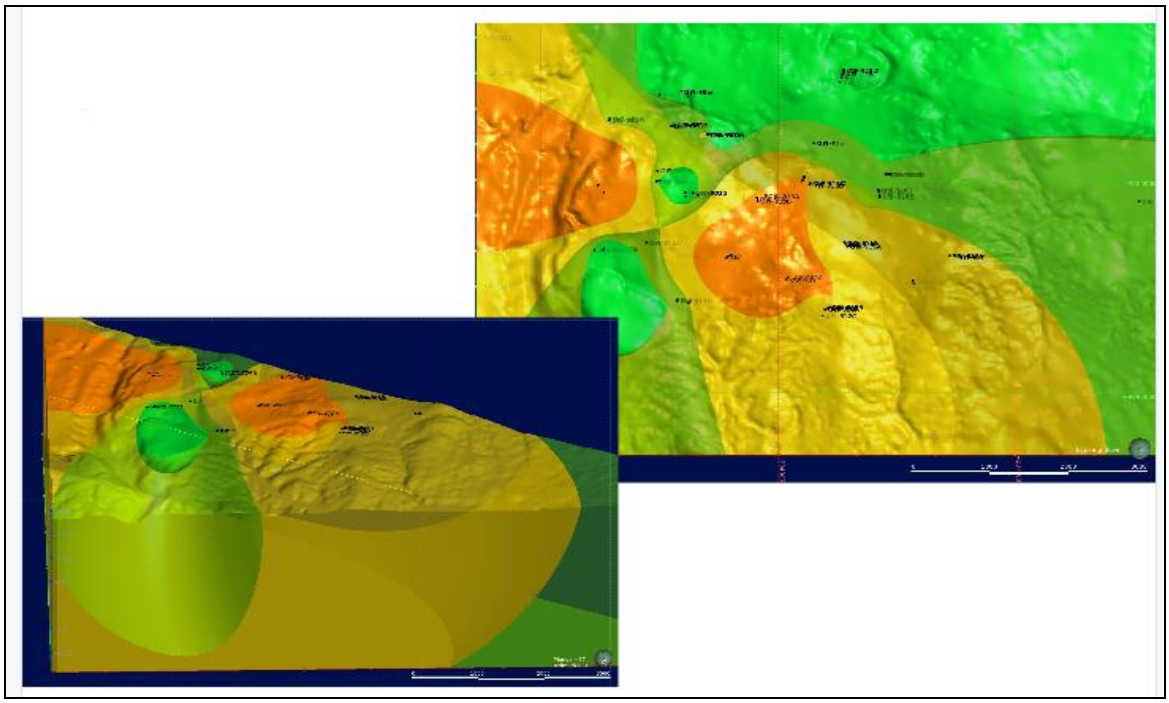

Figure 8: Deep Liquid Chloride Distribution

2.1.6 **Reservoir Data**

Reservoir temperatures for 49 wells were used Data considered are the initial/natural state temperature conditions. The wells underwent heat up periods before they were discharged. Measured temperatures including BPD curve were used to calculate formation temperature. Enthalpy was also determined at wellhead during well discharge production testing where geothermal fluid is passed through orifice.

3.0 Temperature and Conceptual Model

Approached used to produce the temperature model was described by Stimac and Mandeno (2016). Characteristic patterns in each major data set (geochemistry, resistivity, volcanology, structural geology) were used together to infer plausible conceptual model elements and reservoir temperature. Since the temperature distribution is related mainly to convective circulation, it indicates flow paths and sources, as wells system edges and boundaries. Hottest areas are likely regions of upflow whereas anomalously low temperatures may indicate downflow of cooler fluids. Overturns of temperature typically indicate tabular outflow sheets. Conductive temperature profiles indicate insufficient permeability to hydrothermal circulation. Overturns or strongly conductive profiles were generally not observed in Domes well data.

3.1 Hard Data

Deep wells were drilled from essentially 26 locations, with about 21 being reviewed in this study (Figure 9). Most of the original wells were vertical, whereas later wells were mainly drilled directionally. It was noted that in the temperature profiles provided for the model, some significant temperature differences were observed with depth in wells drilled from the same location. This introduces one the main uncertainties in the model, and deserves further refinement based on integration of additional data, and update with the latest interpreted temperature data. It is suspected that some of the profiles of the most recently drilled wells were not fully stabilized, but it is also possible that some wells intersected cool downflows controlled by near-vertical faults.

For purpose of describing the patterns of reservoir temperature, the field was divided into sectors, each 2 x 3 km ($9km^2$) about a central location at 204000E and 9900000N (Figure 9)

Based on the shape of the input temperature profiles, wells were classified in as:

1) Outfield wells with relatively low conductive gradients;
2) Edge wells with high, nearly conductive gradients;
3) Outflow wells with a shallow temperature maximum, followed by a reversal;
4) Upflow wells with high convective profiles resembling a two-phase gradient;
5) Infield wells with high convective profiles with no reversals.

Most wells were Upflow or infield wells with either high convective temperature profiles with no reversal with depth. Only a few edge wells had low temperature, although even these generally had convective profiles.

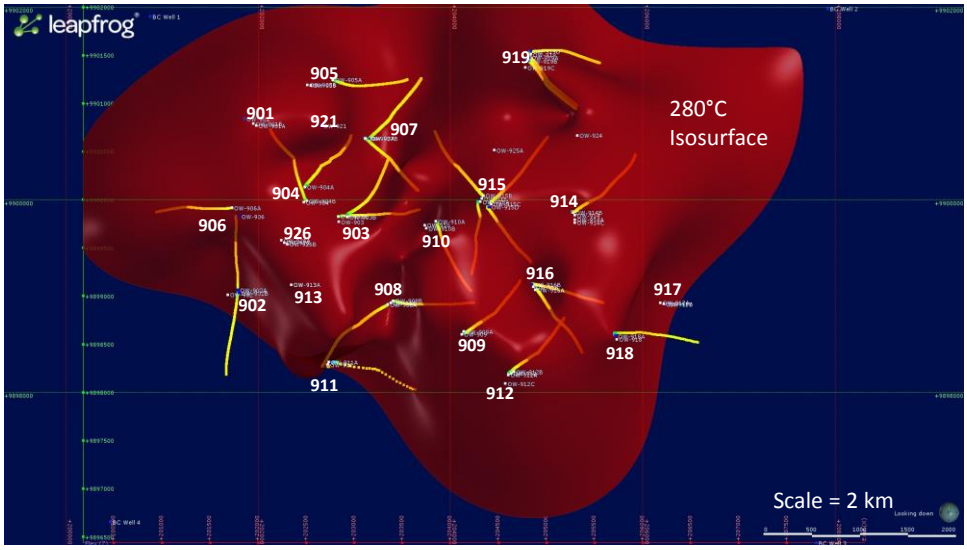

Figure 9: Map view of well sites and temperatures (colors along well paths) and interpolated 280°C isosurface (red). This view shows that most wellsites have two or more wells directional wells.

3.2 Boundary Conditions and Soft Data

Temperature model is populated by 49 deep wells. Boundary conditions are specified by four (4) control wells at the project boundaries (BC-1 to BC-4) at the far corners of the model. All four control wells have nearly isothermal profiles to 500 m depth, then have conductive gradients of 80°C/km from 500 m to 3500 m vertical depth. The low shallow gradient is input to simulate a nearly constant temperature in an unsaturated zone above a deep water level that is commonly observed throughout the area. The relatively high conductive gradient is typical of the impermeable margins of many geothermal areas worldwide. Higher gradients (100-140°C/km) are common at the immediate edges of active convective circulation systems, but were not employed in this study.

Previous studies showed that wells OW-915, OW-909, OW-909A, and OW-910A (SE sector) had high temperature and pressure, and relatively high chloride indicative of a region of upflow (e.g., Mwarania, 2010; Kanda, 2011a; Rop, 2012). A smaller high was also indicated by OW-904B (NW sector). Wells OW-903B, OW-905A and OW-907A, OW-907B are generally cooler on comparison between formation temperature and alteration mineralogy.

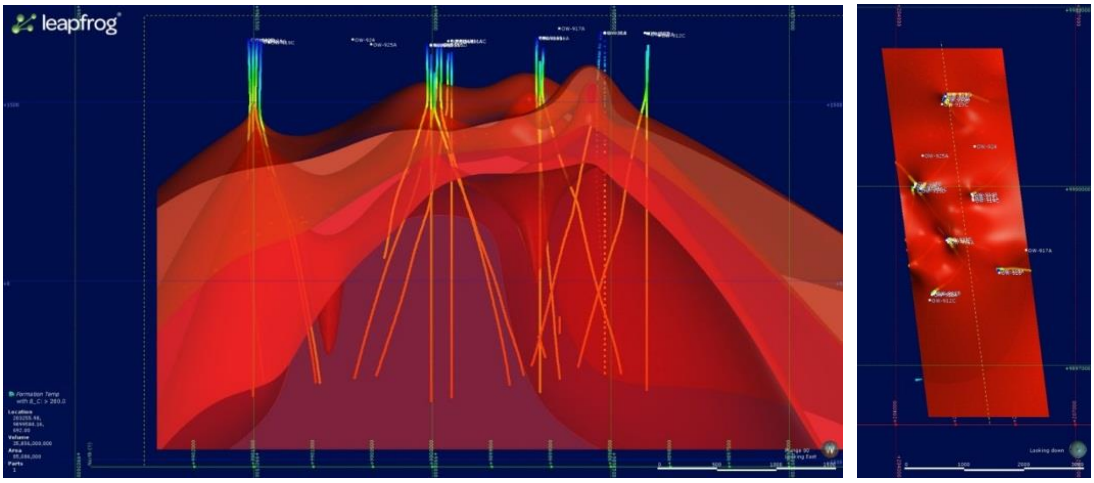

Figure 10: Approximately N-S 3D slice extending from OW-919 to OW-912 locations looking E.

Interpolated temperature model from this study suggests two regions of upflow, separated by a narrow saddle of lower temperature. The main upflow, in the SE near arcuate dome vent areas, has been highlighted in previous studies, and represented by wells OW-909, 912, 914, 915, 915A, 915C, 915D. A smaller area of high temperature is located in the NW, represented by wells such as OW-901, 921, 904B. The area of lower temperature may be related to the presence of cooler downflow, a barrier to flow, or a low permeability zone. It is represented by wells such as 903B, 904A, 905A, and 907A, 907B. It occurs near vents and feeder dikes of the Plateau domes, and intersections of NE and NW-trending structures that may allow deeper ingress of cool fluids. The reservoir appears to have relatively sharp boundaries on the S (OW-902B, 911, 911A), SE (OW-917, 918A) and NW (OW-919D) Figure 10.

CONCLUSION AND RECOMMENDATION

Use of Leapfrog Geothermal has made it possible to create a 3D model of Olkaria domes. It has provided an opportunity to integrate various data types; geology, GIS geochemistry, geophysics and reservoir well test measurements. It has created a better understanding and visualization of the controls on fluid flow within the reservoir. It should be noted this is work in progress and that the model shown here is considered preliminary. It can be considerably refined by addition of new data, and more detailed review of well temperature profiles, flow rates, enthalpy, and geochemistry. Review of well flow, enthalpy and geochemistry with time should also provide insight to flow paths in the reservoir and sources of recharge as production is increased and the reservoir pressure drawn down.

In progress also is extension of the model to the other sectors of Olkaria geothermal field so that we obtain a wholistic visualization of the Olkaria geothermal model using Leapfrog Geothermal software.

4.0 REFERENCES

Arnórsson and Bjarnason, 1994, Speciation program WATCH, Version 2.1 Orkustofun, Reykjavik, 7pp

Atieno, O.J., 2011, Hydrothermal alteration mineralogy of Well OW-914, Olkaria Dome Field, Kenya.Proceedings, Kenya Geothermal Conference 2011 KICC, Nairobi, November 21-22, 2011.

Clarke, M.C.G., Woodhall, D.G., Allen, D., Darling, W.G., 1990, Geological, volcanological and Hydrogeological controls on the occurrence of geothermal activity in the area surrounding Lake Naivasha, Kenya.Ministry of Energy, Nairobi, Kenya, BGS Report, 138 pp.

Giggenbach, W. F 1988, Geothermal solute equilibria, derivation of Na-K-Mg-Ca geoindicators. Geochem. Cosmochim, Acta, 37, 515-525

Kanda, I., 2011a, Conceptual Model Based on Preliminary Observation of Ongoing Geothermal Resource Appraisal at the Dome Wellfield, Olkaria, Kenya. GRC Trans. 35, 1467-1473.

Kanda, I., 2011b, Aquifer Fluid Chemistry Characteristics for the Dome Geothermal Wellfield, Olkaria, Kenya. GRC Trans. 35. 631-635.

Lagat, J., Arnorsson, S., Franzson, H., Proceedings World Geothermal Congress 2005. Antalya, Turkey, 24-29 April 2005.

Lagat, J., 2010, Successful use of hydrothermal alteration mineralogy in appraising a geothermal reservoir: case study -Olkaria Domes, Kenya. Proceedings, 3rdARGeo Conference, Djibouti, 2010.

Lichoro, C.M., 2009, UN Geothermal Training Programme 2009-16, Joint 1-D inversion of TEM and MT data from Olkaria Domes Geothermal Area, Kenya.

Malimo, S.J., 2009, Interpretation of geochemical well test data for wells OW-903B, OW-904B and OW-909 Olkaria Domes, Kenya. UN Geothermal Programme Report 2009-17, 319-344.

Marshall, A.S., Macdonald, R., Rogers, N.W., Fitton, J.G., Tindle, A.G., Nejbert, K., Hinton, R.W., 2009, Fractionation of Peralkaline Silicic Magmas: the GOVC, Kenya Rift Valley. J. Petrol. 50, 323-359.

Mungania, J., 1992, Surface geology of Olkaria- Domes field. KPC, unpublished. Internal report.

Mwarania, F.M., 2010, A reservoir assessment of the southeast part of Olkaria Domes Geothermal Field, Kenya. UN Training Programme Report 2010-22.

Opondo, K.M., 2008, Fluid characteristics of three exploration wells drilled at Olkaria Domes field, Kenya. Proceedings 33rd Workshop on Geothermal Reservoir Engineering, Stanford University, 6 pp.

Rop, E., 2012, Results of Well Production Test for Olkaria Domes Field, Olkaria Kenya. Proceedings 4thARGeo Conference, Nairobi, Kenya.

Stimac, J., Mandeno, P.E., 2016, A Workflow for 3D Geothermal Conceptual Models– Moving Beyond the Flat Cartoon, Transactions Geothermal Resource Council.

Ussher, G., Harvey, C., Johnstone, R., Anderson, E., 2000, Understanding the resistivities observed in geothermal systems. Proceedings World Geothermal Congress 2000.